Validation of a District Heating System Model and Simulation-Based Investigation of Bidirectional Heat Transport by Decentralized Solar Thermal Plants

Daniel Beckenbauer[1,2], Mathias Ehrenwirth[1,2], Michael Klärner[1], Wilfried Zörner[1] and Vicky Cheng[2]

[1] Institute of new Energy Systems, University of Applied Sciences Ingolstadt (Germany)

[2] Munich School of Engineering, Technical University of Munich (Germany)

Abstract

This work discusses a MATLAB/Simulink-based modelling approach for the simulation of bidirectional flow in district heating systems with decentralized solar thermal plants. Based on the results of a monitoring campaign of an operational district heating network with decentralized solar thermal plants, a simulation model of the system is validated. Modified components for pipes, thermal storages and network junctions are derived from the CARNOT toolbox and additionally validated by laboratory tests. These components are used to enhance the model for the simulation of a reversed flow in the district heating pipes. Based on this modification, a study is conducted to examine the performance of a return-supply feed-in compared to a return-return feed-in for different dimensions of solar thermal plants in the network. The comparison shows that for small plant sizes and low solar fractions, a pure return-return feed-in can be suitable, whereas for higher solar fractions, a return-supply feed-in increases the solar yield of the decentralized plants.

Keywords: district heating, modelling, bidirectional flow, decentralized solar thermal plants

1. Introduction

The integration of solar heat into district heating systems is a promising approach for the reduction of carbon dioxide emissions from domestic hot water and space heat consumption in urban areas. While large contiguous collector arrays are a cost effective way of supplying newly built areas and large ambitious renovation projects with solar heat, existing buildings and district heating networks in densely built-up quarters require adapted solutions to deal with the limited space. The decentralized integration of solar collectors and diurnal heat storages is one possible answer to this challenge. However, as this approach transforms the connected buildings from pure consumers to prosumers, a detailed planning of the design and operation of multiple plants interacting in one energy supply system is required. The simulation-based optimization of the hydraulic layout, the dimensioning and the control strategy is an essential step towards the realization of such projects.

Four major hydraulic schemes can be identified for the decentralized integration of solar heat. These are return-return (RR), supply-return (SR), supply-supply (SS) and return-supply (RS) feed-in (Schäfer et al. 2014). While the first three concepts do not lead to a change in the flow direction of the water circulating in the district heating pipes, the RS feed-in causes a reversed flow in the branches where decentralized heat generators are in operation. This operation mode is shown in Fig. 1, where the upper scheme represents the flow distribution when the central heating plant is the sole heat supply. The bottom scheme shows the same system while a decentralised heat generator is additionally active, which allows partly supplying other consumers in the system with the necessary nominal flow rate. While this feed-in strategy is very attractive due to the parallel operation of decentralised heat generators on the same supply and return temperature level as the central heating plant, it is on the other side more complex in terms of hydraulic layout and system operation. In some existing systems, additional solar pipes are used in parallel to the district heating supply and return pipe, allowing additional hydraulic design parameters (so called 2+1 or 2+2-systems). Examples can be seen in Mies and Rehrmann (2007) or Paulus and Papillon (2014). However, this leads to additional costs. Furthermore, for most existing district heating systems, it may be difficult to add another pipe in the ground. As this paper aims at renovation projects, this approach is not further discussed and the connection of the solar thermal plants to the existing district heating pipes is the focus of the work.

doi:10.18086/swc.2017.06.01 Available at http://proceedings.ises.org

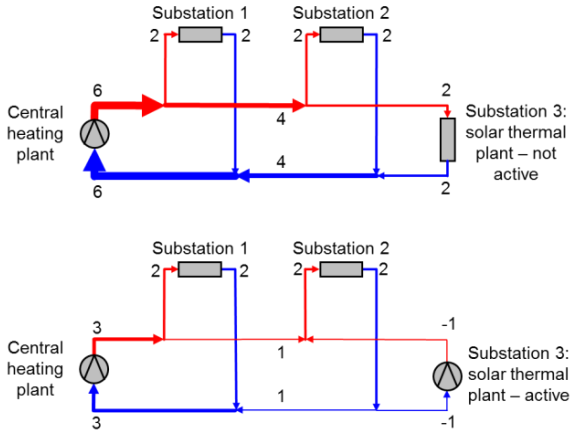

Fig. 1: Change in flow conditions during activation of a decentralized RS feed-in. Top scheme: solely supplied by central heating plant; bottom scheme: additional decentralized feed-in by solar thermal plant (numbers show nominal flow rates)

The CARNOT-toolbox in MATLAB/Simulink provides a block library with all necessary components to model heating systems – including district heating – for the conceptual design of these systems (Hafner et al. 1999). Due to the unidirectional information flow between Simulink blocks, it is, nevertheless, not straightforward to model the reversed flow in pipe connections between components like boilers, storages and heat exchangers. A modification and extension of the available CARNOT library is, therefore, necessary to enable the design of a district heating system with decentralized solar thermal plants utilizing an RS feed-in. One approach of such a modification is presented in this paper, validated by measurements and tested in a district heating network model.

2. Description of the existing district heating network

The basis of the system simulation is the metrological investigation of an existing, operational district heating network in Ingolstadt, Germany, which is shown in Fig. 2. The network was built in the 1970´s and was equipped with four decentralized solar thermal plants in 2016. It was decided to use single-cover flat-plate collectors in this case, to keep the investment costs on a low level. The standard CARNOT toolbox was used for designing this renovation project and all plants were equipped with comprehensive metrological equipment to measure the temperatures and volume flows in the systems as well as the heat flows in each branch continuously. While three plants have the same collector area of 71 m² and orientation, the hydraulic integration concepts differ. The similar sizing allows a comparison of the different utilization concepts:

- One solar thermal plant was installed on the roof of the main building (Hindenburg 57 – HB57), where the central heating plant is located. As the building has 85 residential units and, therefore, a high domestic hot water consumption, there is no need to feed in heat from the solar thermal plant into the network. Due to the high ratio of heat consumption to collector area and the resulting low operation temperatures, the plant can achieve a high annual yield of 42.5 MWh at the average local climate.
- Another system (Hindenburg 36 – HB36) is designed for pure feed-in and is very simple regarding the hydraulic layout and the control strategy. In addition, it has only small space requirements in the building, as it does not require a thermal storage, making it easy to integrate into the existing quarters. The feed-in strategy is a pure RR feed-in. The plant is directly connected via a plate heat exchanger to the main return pipe of the network passing by the building. Measurements show an average annual yield of 16.9 MWh at the current operation parameters of the network.
- Finally, there are two systems for a combined use, meaning that in a first step the solar heat is consumed directly in the building for domestic hot water preheating. Only if there is excess heat and the storage temperature reaches a certain level, the feed-in to the return of the network is activated. The plants achieve an annual yield of 26.6 MWh for the south oriented roof (Schubert 21 – SB21) and 31.8 MWh for the west oriented roof (Schubert 12 – SB12), where 21 m² vacuum tube collectors are additionally in operation. These collectors were already installed and integrated to the new plant. Local solar fractions for domestic hot water of the two plants are 73 % and 49 % respectively. During summer, this fraction increases up to monthly values of 140 %. The installed excess heat feed-in reliably transfers the heat into the district heating return.

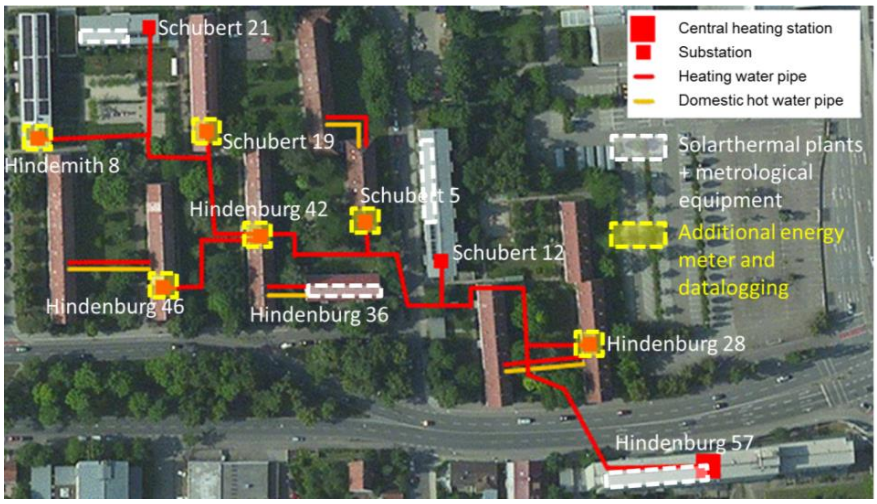

Fig. 2: Scheme of the existing district heating network with decentralized solar thermal plants

3. Description of the simulation model

Fig. 3 shows the layout of the complete district heating network model. The single components used in this model are introduced in the following section.

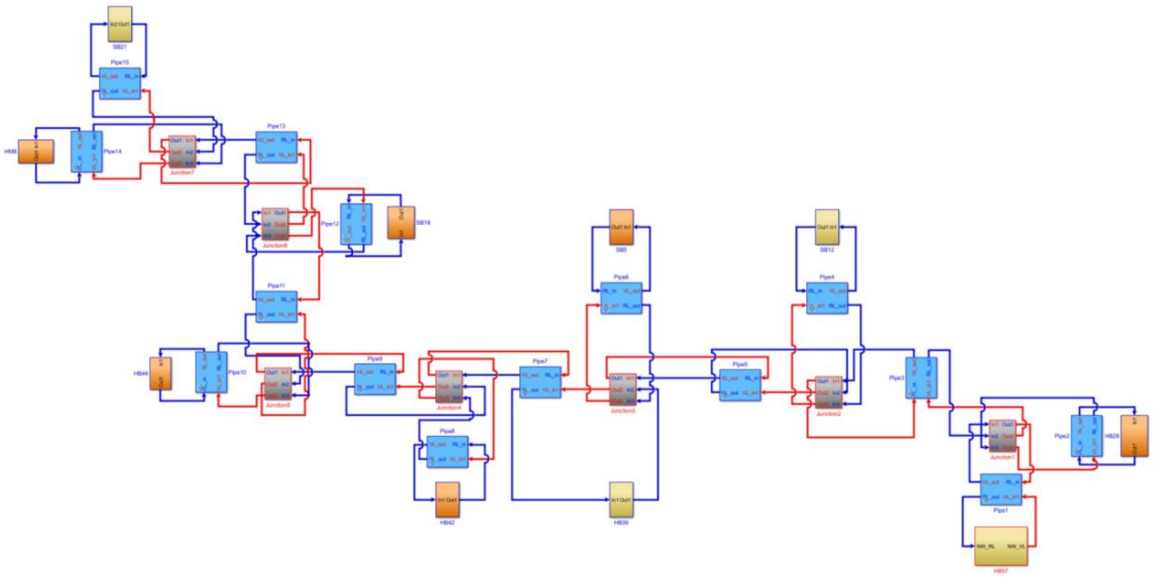

Fig. 3: Depiction of the district heating network simulation model with consumers (orange), producers/prosumers (yellow), pipes (blue) and network junctions (grey)

3.1 Pipe model

For the simulation of a district heating network with decentralized feed-in, four properties of the pipe model are particularly of interest:

- Calculation of the heat losses
- Calculation of the stored energy due to the thermal capacity of pipe and fluid
- Calculation of the time delays of the fluid flow in the network
- Ability to simulate a reversed flow in the pipe

To cope with these demands, a new setup of pipe model was developed based on Simulink. As the buildings and other system components are modelled in CARNOT, the thermo-hydraulic vector (THV) was the basis for the new calculation procedure. Besides the temperature and the mass flow, the THV contains several data, which are not relevant to the energy balance of the district heating network and can be simplified without losing accuracy in

this application. As the fluid is always pure water and pressure loss calculations are only of interest for the detailed system design but not for the conceptual layout and control strategy, only the temperature and the mass flow were selected and structured in a 2-component vector for all calculations in the network. To realize the reversed flow in Simulink, the pipe model consists of a *Supply*- and a *Return*-pipe, merged in one block. Fig. 4 shows the structure of this block. It is connected via the *Supply_in*, *Supply_out*, *Return_in* and *Return_out* ports to the superior model. Depending on the sign of the mass flow (positive = heat generation, negative = heat consumption), the *Switch* blocks conduct the information from the *Supply_in* port to the *Supply* pipe and the *Supply_out* port for standard operation. During a decentralized feed-in, the *Return* pipe is connected to the *Supply_in* and *Supply_out* ports to establish the reversed flow. The *Memory* blocks are used to break algebraic loops by adding a one integration step time delay. As the time step is always below 10 s (approximately 3 s in average), this does not lead to a significant error in the simulation.

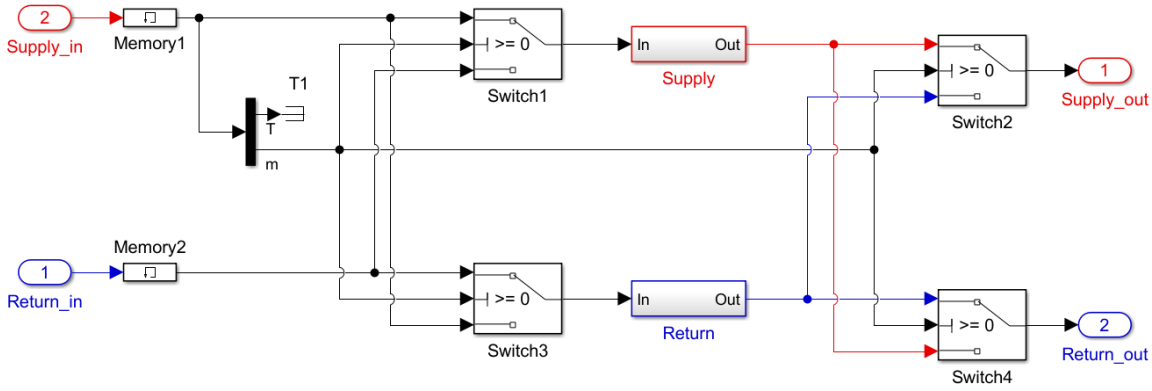

Fig. 4: Pipe block with *Supply* and *Return* pipe and *Switches* for change of the flow direction

Inside the *Supply* and *Return* blocks, several calculations are performed to emulate the pipe behavior (Fig. 5). The *Delay* sub-model takes the current mass flow of the fluid in the pipe, calculates the fluid velocity and, based on the pipe length, the transport delay from the inlet to the outlet. The temperature information at the inlet is then kept for the calculated delay duration until the fluid is conducted to the *Q_loss* and the *E_pipe* block. These blocks represent the energy balance at the pipe (losses through insulation, stored internal energy due to fluid, pipe wall and insulation capacity). Integrating the sum of these two terms after multiplication with the total pipe capacity leads to the time-dependent outlet temperature. The same calculation is performed in the *Return* pipe of the block.

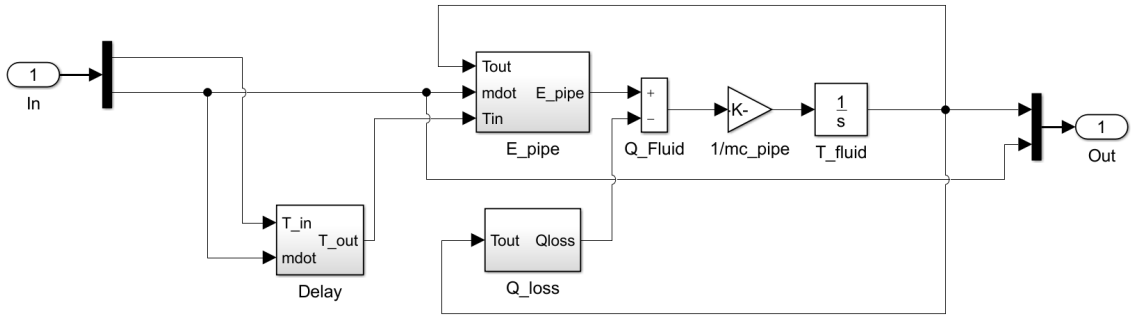

Fig. 5: Layout of a single pipe component with time delay, energy loss, energy balance of inlet and outlet and thermal node of the pipe

Some simplifications are introduced in this pipe model. Firstly, the heat capacity of the water is assumed to be constant at 4,188 J/(kgK). This is justified as the maximum deviation of the real value within the temperature range between 0 °C and 100 °C is less than 0.5 %. Secondly, the temperature of the pipe wall is assumed to be the same as the fluid temperature, which is acceptable if the thermal resistance of the pipe insulation is much higher than the thermal resistance of the pipe wall and the convective heat transfer between fluid and pipe wall. For thermal conductivities of the insulation material around 0.04 W/(mK) and thicknesses in the range of the pipe diameter, this assumption is sufficient. For the calculation of the insulation capacity, an average insulation temperature has to be defined. This results from the fact that when assuming a linear temperature gradient along

the insulation thickness, more than half of the insulation material mass is closer to ambient than to fluid temperature due to the increasing lateral surface at larger distances from the pipe wall. For a pipe with an insulation thickness equal to the inner diameter, this results in a weighted temperature of 37 % of the inner temperature compared to ambient, meaning that e.g. at 80 °C fluid and 20 °C ambient temperature, the average insulation temperature is only at 42 °C. To cope with this fact, 37 % of the total capacity of the insulation are added to the fluid capacity and set to fluid temperature whereas the other 63 % are neglected. Fig. 6 illustrates this correlation.

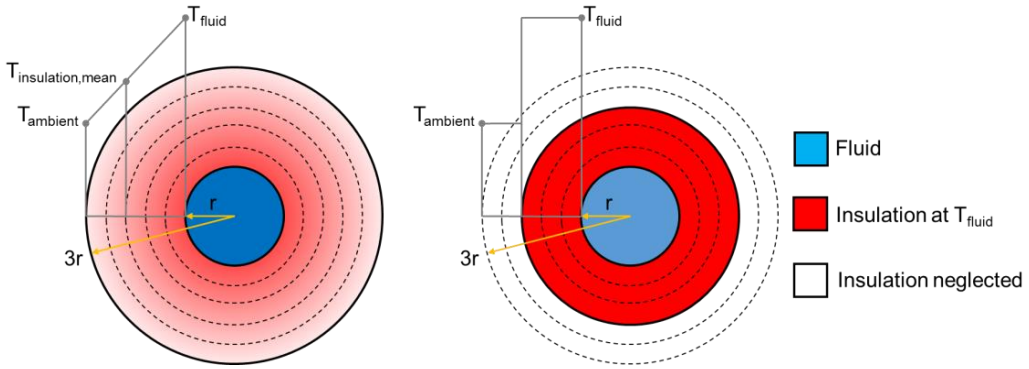

Fig. 6: Real (left) and discretized (right) temperature distribution across the pipe cross-section with equal stored energy

As the thermal conductivity of insulation materials can be highly dependent on the temperature, a temperature-conductivity function is introduced using a set of temperature-conductivity pairs and a linear interpolation between the known values. Equation 1 gives the heat loss of the pipe:

$$loss = \frac{2 \cdot \pi \cdot l}{ln\left(\frac{D+\frac{2 \cdot P_i}{100}}{D}\right)} \quad \text{(eq. 1)}$$

The thermal capacity of the fluid, the pipe wall and the insulation can be calculated by:

$$mc_f = l \cdot \frac{D}{2} \cdot \pi \cdot \rho_f \cdot c_f \quad \text{(eq. 2)}$$

$$mc_w = l \cdot D \cdot \pi \cdot t_w \cdot \rho_w \cdot c_w \quad \text{(eq. 3)}$$

$$mc_i = l \cdot \left[(0.5 \cdot D + \frac{D \cdot P_i}{100})^2 - (0.5 \cdot D)^2\right] \cdot \pi \cdot \rho_i \cdot c_i \quad \text{(eq. 4)}$$

The delay time of the fluid particle and temperature information between inlet and outlet of the pipe is given by:

$$delay = \frac{l}{\frac{\dot{m}}{\left(\frac{D}{2}\right)^2 \cdot \pi \cdot \rho_f}} \quad \text{(eq. 5)}$$

The change of the internal energy of the fluid in the pipe is:

$$\dot{E}_{fluid} = (T_{in} - T_{out}) \cdot c_w \cdot \dot{m} \quad \text{(eq. 6)}$$

With the change in internal energy and the loss, the new outlet temperature of the pipe can be calculated by:

$$T_{fluid} = \int \frac{1}{mc_{fluid} + mc_{wall} + 0.37 \cdot mc_{insulation}} \cdot (\dot{E}_{fluid} - \dot{Q}_{loss}) \delta t \quad \text{(eq. 7)}$$

With:

$\dot{m}$	*mass flow in the pipe*	*kg/s*
$mc_{w,\,f,\,i}$	*mass times thermal capacity of the pipe wall, fluid or insulation*	*J/K*
l	*length of the pipe*	*m*
D	*inner diameter of the pipe*	*m*
t_w	*wall thickness of the pipe*	*m*
P_i	*relative insulation thickness based on pipe diameter*	*m*
$\rho_{w,\,f,\,i}$	*density of the pipe wall material, fluid or insulation*	*kg/m³*
$c_{w,\,f,\,i}$	*specific thermal capacity of the pipe wall material, fluid or insulation*	*J/(kgK)*

Another simplification is to define the pipe as a one-node capacity along the pipe length. This results in the fact that a temperature gradient along the pipe length cannot be simulated in detail. In addition, the heating and cooling process of the pipe wall and insulation are neglected, as the temperature of these parts is assumed to be immediately at fluid temperature.

3.2 Network junctions

A dedicated *Junction* component is used for the pipe couplings of the network. As at every point in the network, there is a supply and a return temperature, this component has an “upper” and a “lower” node, representing these temperatures. The upper temperature is calculated as the mass-flow-weighted mean value of all incoming supply flows, whereas the lower temperature represents the mass-flow-weighted mean value of all incoming return flows. The decision of whether an incoming flow is directed to the upper or lower node depends on the sign of the mass flow. Similar to the pipe supply and return component, this is performed by *Switch* blocks in the *Junction*. As on the network level, the mass flows are calculated in a bottom-up approach from the single buildings back to the flow at the central heating station, the flow in branch one, connected to the junction is the sum of branch two and branch three. Fig. 7 shows the junction sub-model.

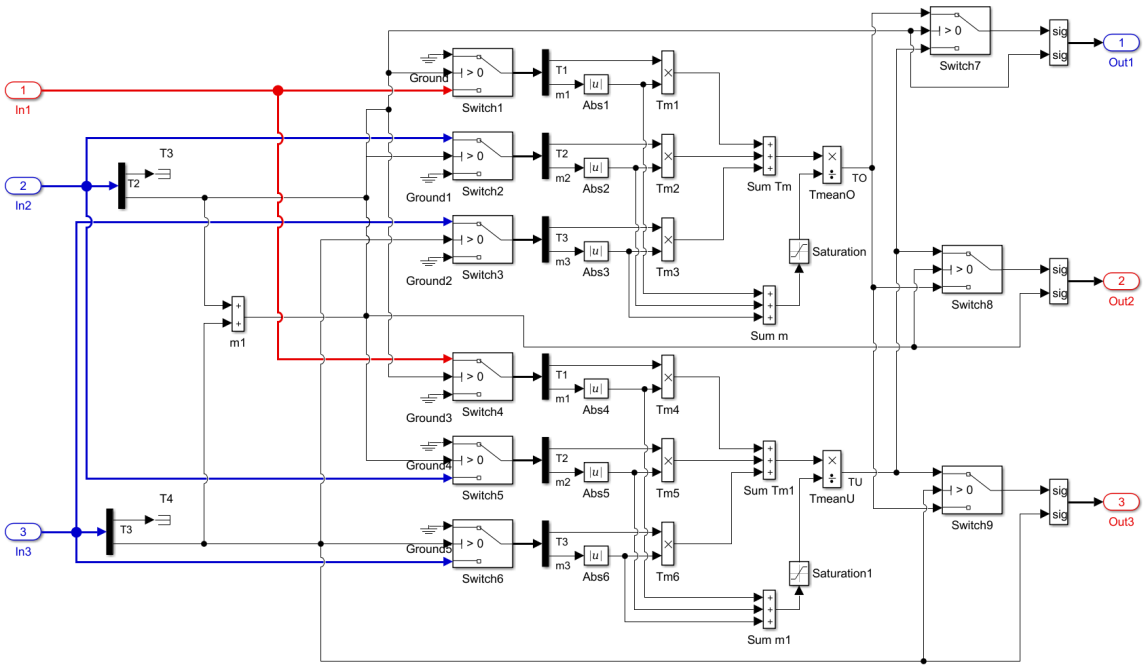

Fig. 7: Sub-model of a network junction

3.3 Substations

The connection of the modified network model to the CARNOT-based building models is realized by a hydraulic compensator that is based on the CARNOT storage model. Fig. 8 shows the sub-model with the relevant connections for space heating, domestic hot water storage, solar thermal plant and the bidirectional connection to the district heating network. Inside this block, the same *Switch*-based decision is performed like described for the pipe and the junction components, if there is currently a consumption from or a feed into the network. By selecting the storage connection heights either to a flow from top to bottom or vice-versa, the bidirectional flow is implemented.

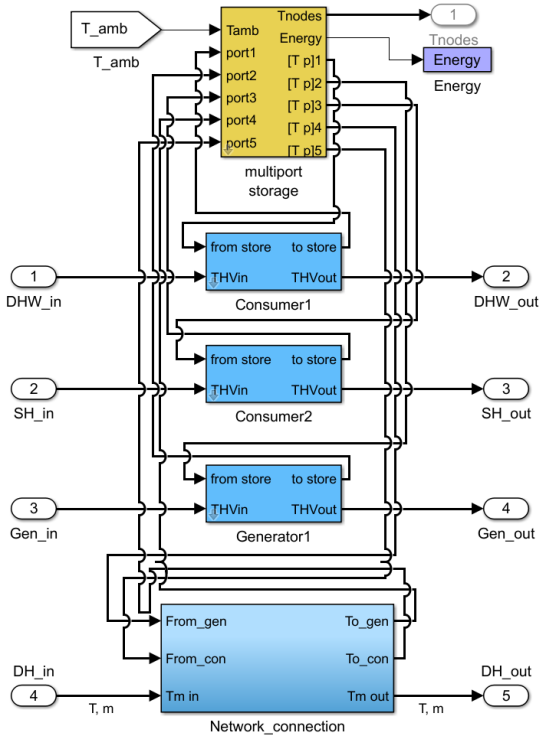

Fig. 8: Substation between modified district heating network model and CARNOT-based building model

4. Validation of the model

4.1 Description of the laboratory test

While the network junctions and the connections between district heating network and buildings can be solved by a purely logical approach, the pipe model includes physical properties, which need to be examined in detail. Due to the choice of a one-node model for the pipe, the question arises of how the pipe performs under a sudden temperature change e.g. caused by a reversion of the flow direction. To answer this question, a laboratory test was set up to validate the pipe model. The layout of the test rig is shown in Fig. 9. Main component of this test was a 2.12 m long copper pipe with an inner diameter of 20 mm and a wall thickness of 1 mm. The pipe was equipped with five thermocouples along the length and insulated with a 19 mm EPDM foam insulation. The parameters of the components are listed in Tab. 1. A computer-controlled thermostat maintained a constant inlet temperature at the pipe. A pump and a motor valve were used to set the volume flow in the circuit. To get an immediate temperature load on the pipe, the heated water was conducted through a bypass tube in the first step (green arrow), while cold water was flowing through the pipe (blue arrow). After starting the data logging, valve 2 and valve 1 were closed while valve 3 was opened and the 3-way-valve 4 set to connect the inlet with the pipe sample and to start the temperature load (red arrow). The temperatures of the inlet and outlet sensors as well as the five temperatures along the pipe and the ambient temperature were logged in a one-second interval. In addition, the volume flow was monitored with a magnetic flow meter (MID).

Tab. 1: Parameters of the laboratory test for validating the pipe model

Length of pipe in mm	2,120
Inner diameter of pipe in mm	20
Wall thickness of pipe in mm	1
Thickness of insulation in mm	19
Thermal conductivity of insulation in W/(mK)	0.04
Temperature sensor inlet / outlet	PT100 4-wire 1/10 DIN
Pipe temperature sensors	Thermocouple type T

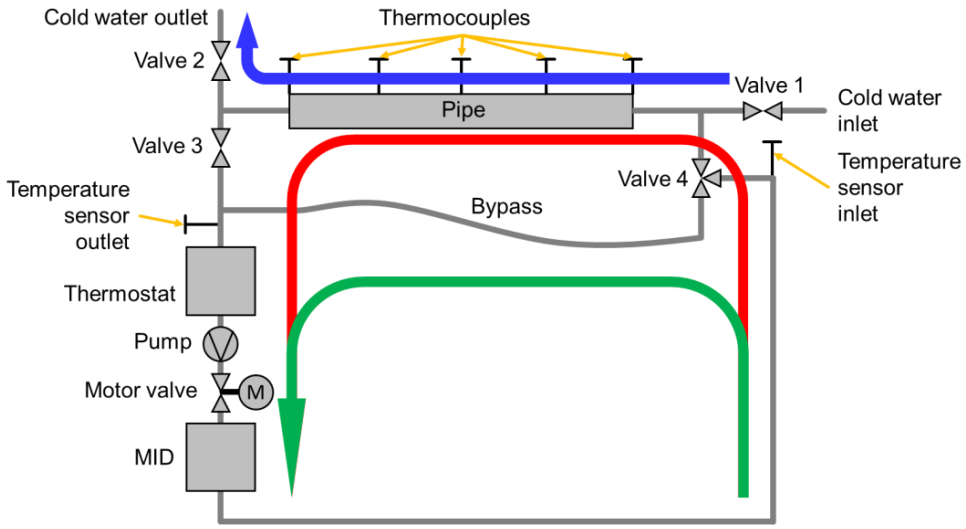

Fig. 9: Layout of the test rig for validating the pipe model

Several measurements were conducted to validate the model at different conditions. The conditions of the presented tests are listed in Tab. 2. In the test *Step Response*, the step response of the pipe was tested at a volume flow of 150 l/h and a sudden inlet temperature change from 22 °C to 47 °C. In the test *Heat Loss*, the pipe was heated up to 70 °C and then the volume flow set to zero to observe the cooling behavior.

Tab. 2: Conditions of the laboratory test for validating the pipe model

Test name	Initial temperature in °C	Inlet temperature in °C	Volume flow in l/h
Step Response	22	47	150
Heat Loss	71	-	0

4.2 Validation of the pipe model

The most interesting results of the first test are the time delay of the temperature change along the pipe length and the shape of the temperature curve after the heating process starts. Fig. 10 shows the comparison of the temperature sensors of the measurement compared with the outlet temperature of the simulation model for the scenario of a sudden inlet temperature increase from 22 to 47 °C. “Tin_measured” describes the measured temperature step at the inlet. “Tout_measured” is the measured value of the temperature at the outlet of the pipe. For the CARNOT pipe, two models were simulated. The first one has only one node (Tout_CARNOT_1). This leads to an instant but slow temperature increase at the outlet. The second model with 100 nodes (Tout_CARNOT_100) describes the time delay very well but shows a too steep temperature increase, when the hot fluid reaches the outlet-node. No node number could be found, where the time delay and the slope of the curve fitted the measured data. For the newly set up model, two variants were simulated, where the first one (Tout_w_I) includes the fractional capacity of the insulation and the second one (Tout_wo_I) only includes the fluid and pipe wall capacity. Due to the fast heating process, the model without insulation capacity fits the measured curve better than the other one. But still, the pipe including the insulation capacity is very close to the measured value and has a more realistic behavior than the CARNOT pipe model in this comparison. The fractional capacity of the insulation was also added to the capacity of the pipe wall in the CARNOT models for better comparison.

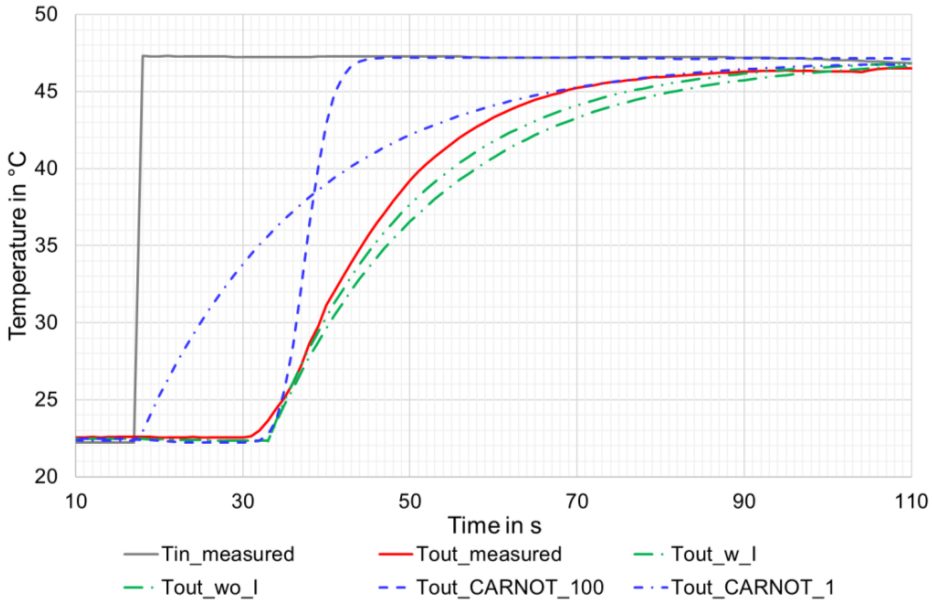

Fig. 10: Temperature curves over time for the step response from 22 to 47 °C

Another important information when discussing the control strategy of the district heating network is the stored energy in the pipes. Fig. 11 shows this energy for the measured pipe, the CARNOT pipe (1 node and 100 nodes) and the new model with insulation capacity. As expected from the faster temperature increase at the outlet, the CARNOT pipe model stores less energy than the measured pipe. The new model calculates slightly higher energies within the period of observation due to the overestimated contribution of the insulation but differs by only 6.3 % in this case.

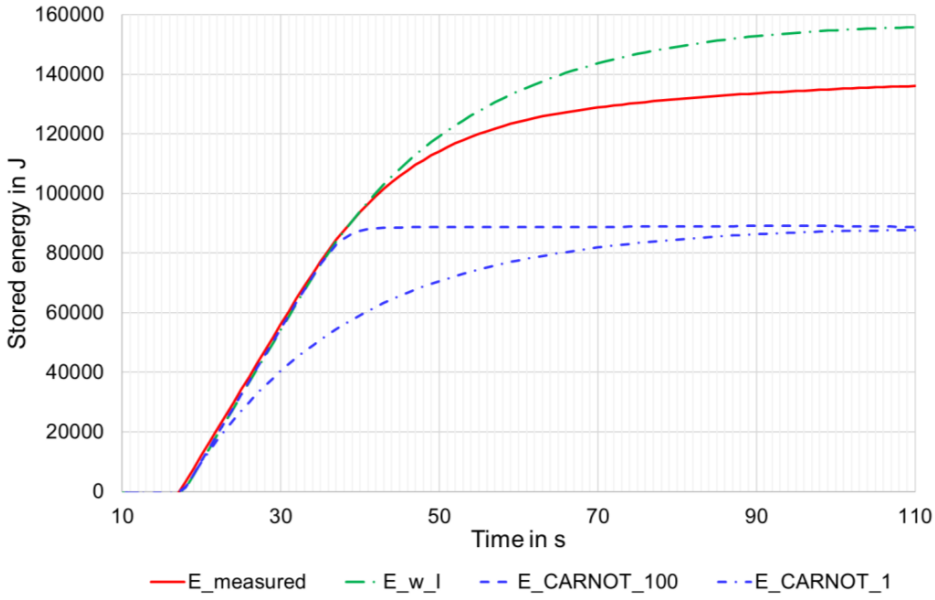

Fig. 11: Stored energy over time for the step response from 22 to 47 °C

The third important point is the calculation of the heat losses in the district heating network. The pipe in the laboratory test was heated up to a constant temperature of 71 °C and then cooled down by the losses through the insulation for approximately 50 minutes. As convection losses in the fluid at the ends of the pipe cannot be completely excluded, only the temperature sensor in the center of the pipe is evaluated. It could be seen that both models are within acceptable tolerance and the temperature loss is 0.8 % too low and 1.7 % too high for the new model and the CARNOT model respectively.

4.3 Validation of the system model

The validation of the complete network model is presented by two exemplary weeks (week 16 and week 20) in 2017. These two weeks represent both, higher and lower ambient temperatures as well as high and average irradiation in the collector plane (Tab. 3). This ensures that sufficient accuracy of the models is achieved under different conditions. The individual components, the overall system and the real control devices were validated in the model. The same collectors and solar stations are installed in all buildings. A distinction is only made in the length of the collector array piping, the array connection and the orientation of the collectors. In addition, the downstream components, e.g. buffer storage, and the connections to the existing local heating or hot water system in the basements are of different designs.

Tab. 3: Average ambient temperature and irradiation on the collector plane for two weeks in 2017

Week	Average ambient temperature in °C	Irradiation on collector plane in kWh/m²
16	4.6	23.9
20	16.1	46.1

In order to be able to make a reliable statement about all different concepts of solar thermal systems, the three different types of installations "local hot water use", "network supply" and "combined solution" are presented using the buildings HB57, HB36 and SB21. Of particular importance are the deviations of solar yields between measurement and simulation over a week, which are defined as follows:

$$Deviation\ in\ \% = \frac{E_{solar,simulated} - E_{solar,measured}}{E_{solar,measured}} \quad \text{(eq. 8)}$$

The measured network temperatures, cold water temperatures and domestic hot water consumption as well as the irradiation in the collector plane and the ambient temperature were set as boundary conditions for the simulations. Tab. 4 shows the results of the metrological investigation and the simulation. It can be seen that the deviations are below 4 % for all considered configurations. Therefore, it can be stated that the accuracy of the model is sufficient for further simulation studies and optimization of the existing network.

Tab. 4: Measured and simulated solar yields for the three plant concepts

	Measurement in kWh	Simulation in kWh	Deviation in %
Solar yield week 16 HB36	253	251	-0.8
Solar yield week 20 HB36	1,033	1,041	0.8
Solar yield week 16 HB57	671	693	3.3
Solar yield week 20 HB57	1,492	1,499	0.5
Solar yield week 16 SB21	386	381	-1.3
Solar yield week 20 SB21	591	611	3.4

5. Simulation study on decentralized feed-in

As the goal of this work is to define a Simulink-based model for the investigation of RS feed-in concepts, a simulation-based comparison based on the operational network is discussed. While in this network, only a RR feed-in could be implemented and the collector area is limited, the simulation model allows additional investigations of the influence of a RS feed-in and larger solar thermal plants. The following designs are compared based on a one-year simulation of the complete network:

- Type 1: Model of the real network and RR feed-in based on CARNOT toolbox
- Type 2: Model of the real network and RR feed-in based on new components
- Type 3: Model of the real network and RS feed-in based on new components
- Type 4: Model with optimized network operation and RR feed-in based on new components
- Type 5: Model with optimized network operation and RS feed-in based on new components
- Type 6: Model with larger collector arrays, optimized network operation and RR feed-in based on new components

- Type 7: Model with larger collector arrays, optimized network operation and RS feed-in based on new components

Type 1 represents the existing, operational network, using only CARNOT components. The operation strategy and the solar thermal plants are designed like in reality. Type 2 is the same but using the modified components for the network. Type 3 is based on type 2 but includes the change from a RR feed-in to a RS feed-in for the plants with combined utilization, while the pure feed-in plant (HB36) keeps the RR concept. Nevertheless, the network operation and plant dimensions are still the same. In type 4, the operation of the district heating system is improved in a way that reduced flow rates are set at the substations to keep the return temperature at an average value of 60 °C during the year, while using a 5 K lower supply temperature during summer. In the existing network, this is not yet implemented but would be possible. Type 4 uses the same RR strategy like type 1 and type 2 but includes a lower feed-in temperature threshold to adapt to the lowered return temperature. Type 5 is again the same as type 4 but with RS feed-in from type 3. Types 6 and 7 contain larger collector arrays as compared to types 4 and 5. The flat-plate-collector areas on the buildings HB57 and SB21 are tripled, as this would still be a feasible design in the existing network. Due to limited roof space, HB36 is kept at 71 m². SB12 has a large available roof area. For these types, the removal of the vacuum tube collectors and a flat plate collector area of 142 m² on the east and 142 m² on the west roof is discussed. This results in a total collector area of the network of 781 m² compared to 305 m² for the other types.

For the simulation study, average climate data for Ingolstadt were used. The thermal loads in the district heating network were derived from measurements of the load profile at the substations in combination with yearly energy consumption data. For the space heat demand, simulations of the buildings were included in the CARNOT model. Tab. 5 shows the solar yields for the plants of all types and their contribution to the heat production of the complete network.

Tab. 5: Annual solar yields and solar fraction of decentralized plants of the simulated system types

Type	Annual solar yield HB57 in MWh	Annual solar yield HB36 in MWh	Annual solar yield SB12 in MWh	Annual solar yield SB21 in MWh	Fossil heat production in MWh	Solar fraction in %
1	42.5	16.9	31.8	26.6	4,289	2.67
2	42.5	16.6	31.1	25.9	4,299	2.63
3	42.5	16.6	31.6	26.2	4,294	2.65
4	42.5	21.2	31.6	26.4	4,261	2.78
5	42.5	21.2	32.4	27.8	4,254	2.83
6	81.2	19.1	57.8	60.1	4,189	4.95
7	79.9	18.8	62.4	70.2	4,165	5.26

Several conclusions can be drawn from the simulation results. Firstly, due to the modified pipe components and resulting variations in the temperatures of the network, there is a difference of the solar yield between the pure CARNOT model and the modified model of 1.6 %. This is considered as acceptable within the scope of this work. Secondly, a RS feed-in has no benefit over the less complex RR feed-in in case of small solar fractions. For the existing network, it increases the solar fraction from 2.63 % to 2.65 %, which cannot compensate for the higher investment costs. The same applies for the existing network with reduced supply temperatures and optimized flow rates. For larger plants, the benefit increases. Type 7 produces 231.3 MWh of solar heat compared to type 6 with 218.2 MWh, meaning an increase of 6.3 %. Thirdly, it can be seen that the pure feed-in concept in HB36 produces less solar heat, when larger plants are connected via RS instead of RR feed-in. This is due to the reduced volume flow passing by the building, when the decentralized plant in SB21 is in operation and supplies the north-west part of the district. Therefore, a combination of the different feed-in concepts is to be avoided. Fourthly, the optimized system operation slightly increases the yield of the plants with partial feed-in but distinctly increases the yield of the pure feed-in plant, which only depends on the return temperature of the network.

6. Conclusions and outlook

For the simulation of district heating networks with decentralized solar thermal plants, a new MATLAB/Simulink-based model was set up. While for the solar thermal plants and the buildings, the standard CARNOT library was used, the network pipes, junctions and substations were modified to allow reversed flow in the network, as is necessary for the simulation of RS feed-in. The pipe model was validated in a laboratory test and shows satisfying performance, which is, in terms of the dynamic behavior of the pipe, closer to reality than the CARNOT pipe. Solar thermal plant models with different hydraulic concepts where validated based on a real district heating network in Germany and also show adequate accuracy. Based on the validated plant and pipe models, a simulation-based comparison was done, showing the difference between RR and RS feed-in for different plant sizes and network operation modes. It can be seen that small plants work well with RR feed-in, which is a simple and reliable configuration for the retrofit of a district. If higher solar fractions are desired, it is beneficial to use RS feed-in to increase the plant performance. Based on the introduced model, further simulation studies will be done to derive recommendations for decentralized solar thermal plants in different districts and to show the possible improvement in performance by an intelligent control strategy for the interaction of the plants.

7. References

Hafner, B. et al., 1999. Carnot Blockset Version 1.0 - Conventional and renewable energy systems optimization blockset - User's guide. Solar-Institut Jülich, Fachhochschule Aachen.

Mies, M., Rehrmann, U., 2007. Abschlussbericht für das Projekt Cohnsches Viertel Hennigsdorf.

Paulus, C., Papillon, P., 2014. Substations for decentralized solar district heating: design, performance and energy cost. Energy Procedia 48, 1076 - 1085.

Schäfer, K. et al., 2014. Dezentrale Einspeisung von Solarthermie in Wärmenetze - technische Analyse von realisieren Anlagen. 24. Symposium Thermische Solarenergie, Kloster Banz, Bad Staffelstein, 7th - 9th May 2014.